POLITECNICO
MILANO 1863

DIPARTIMENTO DI MECCANICA

mecc

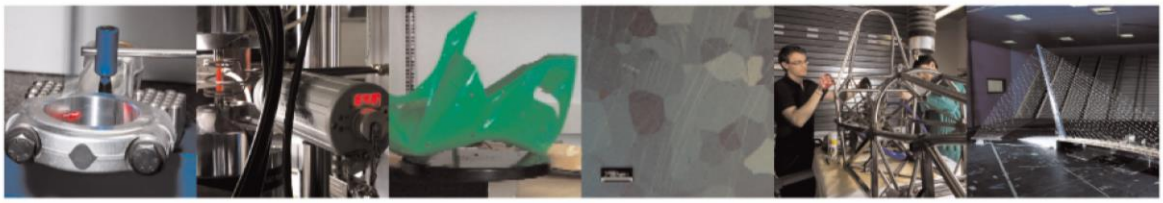

Modelling the conditions for natural convection onset in open-cell porous Al/paraffin composite phase change materials: effects of temperature, paraffin type and metallic structure geometry

Ziwei Li, Elisabetta Garibold

This is a post-peer-review, pre-copyedit version of an article published in journal title. The final authenticated version is available online at:
https://doi.org/10.1016/j.ijheatmasstransfer.2021.121279

Modelling the conditions for natural convection onset in open-cell porous Al/paraffin composite phase change materials: effects of temperature, paraffin type and metallic structure geometry

Ziwei Li[a], Elisabetta Gariboldi[b]

[a]Politecnico di Milano, Department of Mechanical Engineering, Via La Masa 1, 20156 Milan, Italy. E-mail address: ziwei.li@polimi.it (Z. Li). ORCID: 0000-0001-6878-2246

[b]Corresponding author at: Politecnico di Milano, Department of Mechanical Engineering, Via La Masa 1, 20156 Milan, Italy. E-mail address: elisabetta.gariboldi@polimi.it (E. Gariboldi). ORCID: 0000-0002-4443-3495

Abstract

Composite Phase Change Materials (PCMs) can be made combining a PCM, i.e., a material that is able store/release heat by its melting/solidification, and a low-amount of well distributed high-melting and high-thermal conductivity phase with the aim of improving the overall conductivity of the material and keeping its high heat storage capability. The composite made by a paraffin and a porous structure of aluminium (Al) has been considered as the representative of this material class. The design of these materials should not only take into account the melting temperature (T_m) and the volume fraction of the paraffin, but also the geometrical distribution and coarseness of the Al phase, which relate to the effective thermal conductivity of the composite as well as the occurrence of natural convection once the PCM is in the molten state. In the present paper, the inverse Body Centred Cubic (BCC) structure has been confirmed to be the most suitable to model high porosity Al foams. For their BCC modelled structure, an analytical equation is proposed for the evaluation of the overall thermal conductivity of the composite PCMs. Also, new best fit equations for predicting permeability of BBC structure are proposed. Analytical description is also given for the Rayleigh-Darcy number obtained as a product of material-dependent term (related to T_m and volume fraction of PCM) and the geometry dependent term (related to volume fraction of PCM, permeability as well as to material coarseness alternatively given in terms of pores per inch, pore size or unit cell length). The model has been validated by means of literature available experimental data. The proposed simplified model can further be adjusted to correlate the onset of natural convection through the local temperature gradient for the composite PCMs.

Keywords

Composite PCM; Paraffin; Effective thermal conductivity; Permeability; Convection.

1 Introduction

The phase change materials (PCMs) have been employed for thermal energy storage and management in various fields, such as construction, textile, biomedical, solar energy, electronics, batteries [1,2]. The low thermal conductivity of molten PCMs is a typically limiting factor for their use, since it makes slower the thermal response of overall thermal energy storage (TES) systems where PCMs are applied [1,2]. This is for example the case of paraffin waxes, widely applied as PCMs in thermal energy storage systems. Paraffins offer high latent heat fusion with the possibility to select the actual paraffin type on the basis of their melting temperature of interest for the TES system at least in a relatively wide range [3].

The drawback of low thermal conductivity for a PCM material can be avoided by substituting homogeneous PCMs by composite PCMs, where the actual PCM is combined with minor amount of a phase characterized by high thermal conductivity and higher melting temperature [1,2,4]. The high-conductivity phase can be both dispersed in the form of particles [5,6] or a continuous phase [7,8]. Among these latter, metallic porous foams have been reported to have many advantages: (i) the high porosity that can be reached allows high PCM volume fractions and thus high energy storage capacity; (ii) their high surface/volume ratio allows fast heat transfer to the PCM phase; (iii) the metallic structures offer structural functions also when the PCM is completely molten [1,4].

The porous metallic structures, such as for example the complex and disordered foams are usually modelled as lattices, obtained by the regular repetition of unit cells such as the tetrakaidekahedral [9], body-centred cubic (BCC) [9–12], the face-cantered cubic [9,12] ones. In the present study, the BCC structure is considered, as previously suggested to be the closest to real foam [10,11].

In the stage of the composite PCM design, the possibility to have or avoid natural convection of the molten PCMs has to be also taken into account. As a matter of fact, depending on specific part needs and configuration of the TES system, natural convection of PCMs within the PCM composite material can have both favourable and adverse effects. Natural convection in the molten PCM enhances heat transfer during melting process [13], leading to faster responses of the TES system in terms of energy storage/release, as proved experimentally and predicted numerically [14,15]. On the other hand, in the case of possibility for natural convection to take place within a molten medium, the overall thermal response can be effected by the heat source

location [16]. In the case of composite PCMs, this also corresponds to a dependence on the spatial arrangement of composite phases [17,18]. Finally, natural convection phenomena cause orientation-dependent heat transfer which could be unsuitable in some engineering components [18]. Similarly, in the special class of PCM composite such as the nano-encapsulated PCMs (NEPCMs) dispersed in a fluid forming nanofluids with PCM properties, Ghalambaz et al. [19,20] observed the effect of orientation of heat flow as well as changes occurring in charging/discharging and, thus, in the effectiveness the TES system induced by different amounts of NEPCMs.

The effects of natural convection in metallic-foam composites PCM has been investigated by several authors [21,22]. Specific studies focus on the presence/suppression [22,23] or on the impact of natural convection of PCM in porous media or in more complex systems or devices containing these porous system [24]. Zhang et al. [21] presented cases of composite PCMs and service conditions where natural convection effect cannot be neglected although the heat conduction is dominant. Lafdi et al. [25], who experimentally studied the phase change heat transfer process of paraffin in aluminium foams characterized by porosity in 88.4-96.6% range, reported that effect of convection is greater in higher porosity and bigger pore size foams. However, on the basis of experimental or simulated tests, some authors stated that natural convection in molten PCMs has negligible effects. The considered cases were Al foam-PCM with 93.5%-94.5% porosity and pore density of 10 pores per inch (PPI) [26], Al foam-PCM with 80% and 95% porosity and pore density of 20 PPI [27], Cu foam-PCM with the porosity of 90% and pore density of 30 PPI [16]. To the authors' knowledge, no organic view is currently available for the combined effects of phases volume fraction and type, porous coarseness, and orientation on the onset of natural convection in composite PCMs. On the other hand, the effect of orientation, size and local geometry of the container of PCM materials on natural convection have been into account by the research groups of Chamkha [19,28–30].

Fluid dynamic studies related to porous media for different engineering applications (see as example Soboleva [31], Poulikakos et at.[32]) show that conduction heat transfer domain as well as the presence of natural convection are correlated to Rayleigh-Darcy ($\mathbb{R}_D$) number. Specifically, where a porous medium filled by liquid is heated from its bottom, natural convection in the liquid phase occurs above a critical value that is close to 40 [31,33]. Where heat is at a lateral surface, with constant temperature, critical $\mathbb{R}_D$ number decreases to 1 [32]

with a stronger tendency for natural convection to arise and contributing to the overall heat exchange.

The Rayleigh-Darcy number is defined as follows:

$$\mathbb{R}_D = \frac{g\Delta\rho KH}{\alpha_{eff}\mu} = \frac{g\rho\beta\Delta TKH}{\alpha_{eff}\mu} \quad (1)$$

where, H [m] is the specimen height, K [m^2] is the permeability of the structure, μ [Pa*s] is the dynamic viscosity of the fluid phase, Δρ [kg/m^3] is the density difference of the fluid, α_{eff} [m^2/s] is the effective thermal diffusivity of the composite and g [m/s^2] is gravitational acceleration. In the case of a direct correlation between density, temperature changes, and temperature-independent coefficient of volumetric thermal expansion β [1/K] (equal to three times the coefficient of linear thermal expansion), the density difference can be expressed in terms of the temperature difference ΔT [K]. In the case, constant β and the average density ρ are used, the equation modifies as written above. Further, the effective diffusivity of the composite can be substituted by the ratio between its effective thermal conductivity λ_{eff} and the thermal inertia I_{eff}:

$$\mathbb{R}_D = \left[\frac{g\beta\rho}{\mu}\frac{I_{eff}}{\lambda_{eff}}\right] \times (KH) \times \Delta T = M \times (KH) \times \Delta T \quad (2)$$

Eq. 2 can thus be split into three terms: the temperature difference ΔT, a material-dependent term (M) and a purely geometrical term (K×H). By using Eq.2, designers can check if critical $\mathbb{R}_D$ values are exceeded or not on the basis of the geometrical features and properties of the porous metallic structure as well as on the properties of the fluid. Nevertheless, to the authors' knowledge, up to now no simple tool is available for designers in view of the selection of suitable geometrical features for the porous metallic structure (such as coarseness and porosity) that allow the presence/absence of natural convection in a composite PCM where the PCM type has been already identified based on its melting temperature.

Actually, this new approach can be followed by considering that the $\mathbb{R}_D$ index is the product of three terms, as shown in Eq.2. The first multiplying factor (M) relates to the properties of the fluid which natural convection motion can occur (i.e., the PCM in its molten phase) as well as to the properties of the composite. The second factor (K*H) is related to the geometrical features of the structural part of the composite PCMs.

The present paper is aimed at giving an overall view of the roles played by geometrical features of the porous structure (such as structure coarseness, porosity, relative component thickness in

the direction of heat flow) on the presence of natural convection in this molten phase of a composite PCM containing a high-melting porous structure. The present paper is specifically focused on composite PCMs made of a paraffin as active phase characterized by melting temperature T_m and an aluminium porous foam as structural phase, modelled as an inverse BCC lattice. The aim is to give the possibility to calculate the $\mathbb{R}_D$ number by simple but accurate analytical models so that the designer can easily predict if the existence of natural convection in a composite PCM. Even if related to paraffin/aluminium composite PCMs, the paper supplies the method to derive the parameters of interest to estimate conditions leading to natural convection in other composite PCMs containing high-melting porous structures.

2 Modelled geometry of the two-phase structure of composite PCMs

The aluminium open cell porous structure is modelled as a lattice formed by regularly 3D stacked inverse body-centred cubic (BCC) unit cell. This means that aluminium stays in the volume not occupied by spheres in a BCC unit cell where spheres of diameter d are placed at the vertices and in the central points of a cube having side length L (Fig. 1a), also referred as lattice length. The open cell structure is continuous when:

$$\frac{\sqrt{3}}{2}L < d < \frac{3}{2\sqrt{2}}L \tag{3}$$

The extreme cases for the open cell Al structure corresponding to the lowest and highest diameter are shown in Fig. 1b. The smallest diameter d corresponds to the case of tangent spheres and to the highest volume fraction of the open-cell structure. The highest diameter corresponds to minimal cross-sectional area and to the lowest volume fraction of the open-cell structure.

In the modelled composite PCMs, the volume occupied by interconnected spheres is filled by the PCM. Focusing on the PCM phase distribution, the model for PCM composite is often referred as the BCC model [9–12]. The porosity ε of the BCC cell thus corresponds to the volume fraction of the PCM in the composite material. The calculation of the porosity can be easily done when the overlapping of sphere volumes is taken into account. As shown in Fig.1c, there are two types of overlapping spheres, each couple consisting of two equal spherical caps whose single volume can be calculated as:

$$V = \frac{\pi \times h^2}{3}\left(\frac{3}{2}d - h\right) \tag{4}$$

where, h is the height of spherical cap. Two types of spherical caps and two corresponding numbers have to be considered: h_1 refers to the case of overlapping between the central sphere and one centred at a cube vertex (16 in total), h_2 refers to the overlapping of two spheres centred on vertices or the caps falling outside the cube cell (6*2). When d is lower than L, there is no overlap between spheres located in vertices (thus h_2=0). As a result, the porosity (i.e., PCM volume fraction) ε can be computed by following equation:

$$\varepsilon = \frac{\frac{1}{3}\pi d^3 - 16\pi {h_1}^2\left(\frac{d}{2} - \frac{h_1}{3}\right) - 12\pi {h_2}^2\left(\frac{d}{2} - \frac{h_2}{3}\right)}{L^3}$$

$$= \frac{1}{3}\pi\left(\frac{d}{L}\right)^3 - 16\pi\left(\frac{h_1}{L}\right)^2\left(\frac{d}{2L} - \frac{h_1}{3L}\right) - 12\pi\left(\frac{h_2}{L}\right)^2\left(\frac{d}{2L} - \frac{h_2}{3L}\right) \quad (5)$$

where, h_1= (2d- $\sqrt{3}$ L)/4. h_2=(d-L)/2 for d>L (ε is about 0.9395) otherwise h_2=0. Since the length size L will be hereafter considered as the geometry parameter representative of the metallic structure coarseness, the second term of the above equation has been rearranged in terms of cell side length normalized values: d/L, h_1/L and h_2/L.

The range of porosity ε in the model adopted can be obtained by combining Eq.3 and Eq.5, corresponding to 0.6802<ε<0.9945. Within this range, for each ε only one d/L solution of Eq.5 is possible, with d constrained to be positive and the condition for open-cell foam (Eq.3). A set of d/L has been calculated in this way by the authors and is plotted in the Fig.2. It can be observed that d/L almost uniformly increases with porosity before ε is 0.9395, then increase faster. In order to simplify the calculation of d/L, analytical expressions for d/L with ε have been derived by best fitting the dataset of points calculated via Eq.5. The following d/L=f(ε) equations are obtained for h_2 equal to or different from zero, respectively:

$$\frac{d}{L} = 0.4665\varepsilon^2 - 0.2452\varepsilon + 0.8179 \qquad \text{for } 0.6802<\varepsilon<0.9395 \qquad (6)$$

$$\frac{d}{L} = 14.855\varepsilon^2 - 27.639\varepsilon + 13.857 \qquad \text{for } 0.9395<\varepsilon<0.9945 \qquad (7)$$

The coefficient of determination (R^2) is 0.9999 and 0.9902, respectively.

Alternatively, a further best fit equation is derived for the whole porosity range for open cell inverse BCC structure:

$$\frac{d}{L} = 4.969\varepsilon^3 - 11.683\varepsilon^2 + 9.599\varepsilon - 1.825 \qquad \text{for } 0.6802<\varepsilon<0.9945 \qquad (8)$$

The coefficient of determination (R^2) is 0.998.

This latter correlation leads to a maximum relative error of around 0.6% at ε=0.994 and thus can be used when rough estimations of d/L can be considered. All the d/L=f(ε) correlations above (Eq.6 to 8), plotted in Fig.2, are independent from the coarseness of the porous structure, which can be linked both to L and d.

3 Material properties and modelled material dependant term M

Once the geometry of the phases has been defined, the temperature-dependence of thermophysical properties of single phases or the effective properties of the composite PCM of interest for the calculation of the M term in Rayleigh-Darcy number need to be considered.

3.1 Material properties

Following the results of a previous paper by the same authors [34], the density (ρ_{PCM}), specific heat ($C_{p,PCM}$), thermal conductivity (λ_{PCM}) in their molten range for paraffins having the melting temperature (T_m) in the range 290-380K can be easily analytically calculated. Equations allow to calculate the properties on the basis of T_m, that is the parameter on the basis of which a paraffin to be used as PCM is selected, as described in recently work by Li [34].

Among many paraffins available, $C_{18}H_{38}$ or $C_{28}H_{58}$ (melting temperatures 300K and 334K, respectively) have been considered for comparison purposes. Their calculated temperature-dependent properties are compared in Fig.3. It can be easily observed that the specific heat of these molten paraffins can be considered as practically independent on paraffin type. Slight dependence on paraffin chemistry can be noticed for density and thermal conductivity.

The property of main interest for the present paper related to the onset of natural convection is the dynamic viscosity of molten paraffins (μ [Pa*s]). Li [34] suggested that the temperature-dependence of dynamic viscosity can be derived from T_m on the basis of the following couple of equations [34]:

$$\mu = 38.78 \times exp(-18.83(T/T_b)) + 0.01426 \times exp(-4.329(T/T_b)) \quad (9)$$

where, T_b represents the boiling temperature for the paraffinic PCM, related to its melting temperature as follows:

$$T_b = 4.56 \times 10^{-5} \times {T_m}^3 - 0.02611 \times {T_m}^2 + 6.341 \times T_m - 201.366 \quad (10)$$

As shown in Fig.3b, for the two paraffins here considered, strong temperature- as well as paraffin-type dependence can be observed.

In the temperature range of interest for considering the onset of natural convection in the modelled composite, which can be considered to range from the melting temperature of the paraffins to 100K in excess of them, the temperature-dependent thermophysical properties of Al are also given in [34]. For example, the values of properties for pure Al phase are calculated at the melting temperatures of two paraffins (300K and 330K): ρ_{Met} = 2699.6 kg/m^3 and 2693.0 kg/m^3 for $C_{18}H_{38}$ or $C_{28}H_{58}$ respectively, while at T_m of the same paraffins $C_{p,Met}$ is 891.0 and 907.8 J/(kg·K), λ_{Met} is 258.7 and 254.7 [W/(m·K)].

3.2 Effective thermophysical properties

In order to calculate the material-dependent term M in Eq.2, the effective thermal inertia I_{eff} and the effective thermal conductivity λ_{eff} of the composite PCM have to be derived. The effective thermal inertia of a multiphase material containing n different phases can be easily calculated as:

$$I_{eff} = \left(\rho C_p\right)_{eff} = \sum_{j=1}^{m} \rho_j Cp_j f_j \quad (11)$$

where ρ_j [kg/m^3], C_{pj} [J/(kg·K)], f_j are density, specific heat and volume fraction of the jth phase of the m phases [35]. This formulation could allow to consider the PCM phase transition for the composite PCM, where three phases are present. Nevertheless, since in the present paper a completely molten PCM with volume fraction ε is considered, I_{eff} can be simply calculated as:

$$I_{eff} = \rho_{Met} \times C_{p,Met}\,(1-\varepsilon) + \rho_{PCM} \times C_{p,PCM} \times \varepsilon \quad (12)$$

On the contrary, the calculation of the effective thermal conductivity of multiphase materials is not straightforward. As a matter of fact, λ_{eff} is not only a function of thermal conductivity and volume fractions of phases, but also of their geometric distribution. Thus, only rough estimation of λ_{eff} can be obtained by applying the mixture rules for phases distributed in parallel or series, which correspond to the maximum/minimum thermal conductivity values [36]. Several analytical equations have been proposed during the years for dilute second phase inclusions [36] or for regularly arranged continuous phases [37–41].

Fig.4 shows the ε-normalized effective thermal conductivity (NETC) correlations in the whole porosity range for which continuous open-cell structure is possible for (inverse) BCC lattice of the high-conductivity phase (a) and for the high-porosity range (b). NETC obtained by direct simulation (DS) from authors' work [34] for the $C_{18}H_{38}$/Al or $C_{28}H_{58}$/Al composites at the melting temperatures of the paraffins are presented as datapoints (black and red star symbols). The results are close to those calculated in literature using the same approach for $C_{22}H_{46}$/Al,

represented by green star symbols [23]. This is due to very small difference in the thermal conductivity of the paraffins, the ratios $\lambda_{low}/\lambda_{high}$ between the low and high-conductivity phase at the temperatures considered is very close (of about $5.9*10^{-4}$, value that should be modelled when $\varepsilon=1$). Since the same ratio will be closer for different paraffins and temperatures considered in the present paper (not exceeding 480K), the results from DS simulation will be very close to those ones. The same holds good for DS calculated PCM composite formed by combining a paraffin with Cu (for which a thermal conductivity close to 400 W/(m K) is generally reported [43,44] and $\lambda_{low}/\lambda_{high}$ of about $3.8*10^{-4}$ is considered), as shown in purple star symbols. In order to show the slight, but still existing, effect of $\lambda_{low}/\lambda_{high}$, plots in Fig.4 also include the results from DS simulation for air/Al and water/Al composites where Al porous structure is modelled as the BCC lattice [10]. In these cases, the $\lambda_{low}/\lambda_{high}$ are 1×10^{-4} and 28×10^{-4}, for air and water, respectively and results (blue and yellow star symbols, respectively) lie across those for paraffin/metallic structures as reasonably expected. The combination of these results shows that also for thermal conductivity ratios varying of 1 order of magnitude, the effect of their change is smaller than that induced by limited changes in porosity.

The above data are then compared in the same figures with experimental data available in literature for the same combinations of materials and metallic open-cell structures with high porosity (open symbols, where in the plots the same colour is adopted for each combination of phases. These results confirm the slight effect of $\lambda_{low}/\lambda_{high}$, but also show that BCC structures well predict the NETC for composites with a high-conductivity open cell structure (about above 0.93) but overestimate NETC for lower porosity. In the porosity below 0.8, a foam becomes more close-cell than open-cell structure [36].

Other lattice description could be adopted for the metallic open-cell structure of the high-conductivity phase of a composite PCM, such as (inverse) face centred cubic (FCC) or simple cubic (SC). Calculations for their effective thermal conductivity were performed by Rawson et al. [42] adopting a lattice Monte Carlo (LMC) approach (leading to a direction-averaged λ_{eff}). For the $\lambda_{low}/\lambda_{high}$ of the same phases coupled in the composite structure ($C_{18}H_{38}$/Al), the results are plotted with black triangular symbols in Fig.4. Their match with experimental data is suitable only for lower than 0.9, while for high-ε these models clearly underestimate NETC. The better fit of BCC model for high-ε has been reported by some authors to be correlated to the minimum surface-area to volume fraction of BCC corresponding to the physical phenomenon of pore formation in foams [10,11].

Alternative lattice descriptions of the high-conductivity open-cell structure have been proposed in literature. Several authors considered structures made of constant-section bars, leaving free one or a few parameters then identified by fitting experimental results [37–41]. While the approach allows a good description of single cases, specifically at high porosity, their application to paraffin/Al porous foam is proved to result in widely scattered NETC for the high porosity values and in an unacceptably low NETC for $\varepsilon<0.88$. These methods are thus not considered there, and their predictions are not shown in Fig.4.

As an overall result from the comparisons made in Fig. 4a and 4b, it can be observed that at relatively high porosity the BCC description is quite good, for the range of ratio between thermal conductivity used in the DS for paraffin/Al or paraffin/Cu are in a narrow range. While the predictions supplied by BCC model for open-pore structures produced by the conventional methods are not suitable as porosity reduces, BCC remains the lattice with the highest NETC for a given porosity and could thus be considered as the target one in some cases such as the composite PCMs considered in the present paper. Its selection as a reference model has thus been confirmed. The description further allows to consider structure with open cell porosity and relatively high NETC in a wide range of porosity (down to $\varepsilon=0.69$). For this BCC lattice the following analytical description (modified by Hu after Progelhof model [23,46] can be adopted:

$$\lambda_{eff} = \varepsilon \times \lambda_{PCM} + (1-\varepsilon)^{\theta} \times \lambda_{Met} \quad (13)$$

where, θ is a fitting constant, identified as 1.3142 by Hu [23] for a $C_{22}H_{46}$/Al, and as 1.3296 by the authors of the present paper [34]. This latter fitting index has been identified by λ_{eff} results provided by direct simulation (DS) at 2 temperatures (T_m of paraffin and (T_m+100K)) for composite PCMs obtained by combining $C_{18}H_{38}$ or $C_{28}H_{58}$ paraffins with the inverse BCC structures made of Al or Cu with porosity ranging from 0.69 to 0.98.

3.3 Modelled material dependant term M

The values of M have been calculated for the composite PCMs made by combining the Al porous structure with different porosity with paraffins $C_{18}H_{38}$ or $C_{28}H_{58}$ (melting temperatures 300K and 334K, respectively). This Eq.13 has been used together with Eq. 12 for I_{eff}, Eq. 9 and 10 for dynamic viscosity and the following one

$$\Delta\rho_{PCM} = 209.5 \times (\Delta T)/T_m \quad (14)$$

derived from the description of molten paraffin density [34], where Δρ is proportional to the temperature difference. The overall equation for M calculation is the combination of the following and Eq (10) for T_b.

$$M = \frac{F}{\mu} = \frac{\frac{209.5g}{T_m} \times \frac{(\rho Cp)_{Met^*(1-\varepsilon)} + (\rho Cp)_{paraffin^*\varepsilon}}{\left(\lambda_{Met^{(1-\varepsilon)^{1.3296}}} + \varepsilon\, \lambda_{paraffin}\right)}}{38.78 \times \exp\left(-18.83 T/T_b\right) + 0.01426 \times \exp\left(-4.329 T/T_b\right)} \qquad (15)$$

Further, a new variable M' is considered, as the ratio between M at a given temperature and the value of M assumed at the melting temperature of the molten (PCM, paraffin) phase, so that M' can be described as:

$$M' = M/M_{T_m} = (F \times \mu_{T_m})/(F_{T_m} \times \mu_T) \qquad (16)$$

Calculations are performed for temperatures ranging from the melting and boiling one for each paraffin, and the results are shown in Fig. 5a. The strong temperature dependence of M', and thus of M and the effect of the molten composite are clear.

In order to investigate the impact of temperature-dependence of properties included in M, a reference case in which only the dynamic viscosity of paraffin is temperature-dependent, while other properties keep constant their values at the melting temperature of the PCM used is considered. In this case M' is equal to:

$$M'_{T_m} = \mu_{T_m}/\mu_T = \frac{38.78 \times \exp(-18.83 T_m/T_b) + 0.01426 \times \exp(-4.329 T/T_b)}{38.78 \times \exp(-18.83 T/T_b) + 0.01426 \times \exp(-4.329 T/T_b)} \qquad (17)$$

where, as usual, T_b is calculated using Eq. 10.

The term M, and correspondingly the M' value in the reference case is lower than in the case of all temperature-dependent properties. The difference between M' values calculated in the reference case and those in the case where all properties are temperature-dependent appreciably increase with temperature, and slightly increases with ε and with the carbon chain length of paraffin. The temperature dependence of M' given in Fig. 5b for each composite is in the temperature range from T_m to T_m+100K for its melting phase. During this temperature range, M' at different volume fraction clearly overlap. For the two paraffins here considered, the difference between M' values obtained in the reference case and that in the case considering temperature-dependence of all properties is lower than 12% at 100°C above T_m of each paraffin type. In applications where paraffins are used as thermal energy storage media these temperatures can be locally reached only when particularly high heating rates or heat flows are imposed/supplied. Under most cases the impact of temperature on viscosity prevails over the

other factors. In these cases, the material-dependent term becomes the ratio between the porosity and T_m dependent term F_{Tm} and the temperature-dependent term μ_T. The calculation of M_{Tm} can be further simplified considering temperature-independent properties of Al. These latter are derived from their temperature-dependent description given in [34] , considering T= 330K, i.e., an intermediate temperature of the melting temperatures for paraffins in the paraffin/Al PCM composites considered in the referred paper.

$$M(T_m, \varepsilon) = F_{T_m}/\mu_T$$

$$= \frac{209.5g\left(2452990(1-\varepsilon)+778.2\left(6.33\times10^{-3}\,{T_m}^2-1.03\,T_m+1961\right)\varepsilon\right)}{T_m\left(253.9(1-\varepsilon)^{1.3296}+\varepsilon\left(0.07128\left(\frac{T_m}{Tb}\right)^2-0.2056\left(\frac{T_m}{Tb}\right)+0.2348\right)\right)}/(38.78\exp\left(-18.83(\frac{T}{Tb})\right) + 0.01426\exp\left(-4.329\left(\frac{T}{Tb}\right)\right)) \quad (18)$$

4 Calculations of the geometry-related term in $\mathbb{R}_D$ equation

The geometry-related term of $\mathbb{R}_D$ number in Eq. 2 is the product of the height H of Al/molten paraffin composite PCMs and of the permeability K of its open-cell structure. The permeability K can be substituted by the product of normalized permeability K' (a size-independent parameter [12,47]), and the square diameter of the spherical pore. Thus,

$$K = K' \times d^2 \quad (19)$$

In the lattices describing the open-cell structure taken into account in the present paper (BCC, FCC, SC), a first-order correlation exists between d and the cell size L, so that K also is correlated to the square of the lattice side length L^2.

Despois [47] presented a microstructure-based model to estimate the normalized permeability K' of open pore microcellular materials. Ngo and Byon [12] proposed a correlation between K' and porosity ε (ε ranging from 0.1 to 0.9) for closed and open cell simple cubic, BCC, FCC structures. To the authors' knowledge, no description of K'-ε correlation exists for the porosity values exceeding 0.90. Thus, simulated tests have been carried out to provide data for BCC structures with high ε, from which good analytical description can derived.

4.1 Direct simulations for permeability K calculation

This part of the study is aimed at providing data to define the dependence of K from geometrical features in a wide range of porosity ε for an inverse BCC lattice structure. Further, the dependence or independence of geometrical features such as structure coarseness (represented by side length L) or thickness of the porous structure (represented by the number of stacked cells) is also confirmed.

In low velocity range of the liquid paraffin, the permeability K of a porous medium within which it moves can be derived by Darcy's correlation [47], where the average velocity of the liquid (u) depends on the permeability of the porous structure (K) and on the dynamic viscosity μ of the paraffin and its pressure difference (ΔP) between the inlet and outlet surfaces:

$$u = -\frac{K\Delta P}{\mu L}. \quad (20)$$

Thus, permeability K can be derived once u, μ and (ΔP) are known. Direct simulations are performed for the unit BCC cell described in paragraph 2 and shown here in Fig.6 with the boundary conditions used for these simulations in order to consider the cell as part of an extremely high number of stacked cells of porous (Al) structure filled by liquid (paraffin). At the inlet and outlet (on the left and right side of the cell in Fig.6, respectively), a periodic pressure and velocity boundary condition is applied to simulate the situation where the fluid can move across an infinite number of stacked cells in the direction of heat flow, differing only by a pressure offset ΔP in the flow direction. The lateral sides are assigned as the symmetry condition and the no-slip boundary condition is applied to all the solid-liquid surfaces. A steady incompressible flow is assumed, and the Navier-Stokes equations are used to govern the motion of fluids. All the above conditions corresponded to those previously considered by Ngo et al. in [12] to the identification of permeability of porous structures with maximum pore fraction of about 0.84.

From the simulation results, the average velocity of u (averaged on the area framed by the bold red box in Fig.6) is calculated and K is derived from Eq. 20. In DS simulation, ΔP is adjusted to obtain the value of Reynold number (Re) lower than 0.1, since it has been reported that Re has a negligible effect on K when Re is smaller than 10^3 [12].

The DS model is implemented in finite element software, using a cell size L equal to 1mm. Tetrahedral elements are then selected. For selected porosity levels (0.757, 0.85, 0.95), a mesh sensitivity analysis has been performed, keeping element size parameters such as minimum mesh size ($4*10^{-6}$m) and maximum element growth rate defining the maximum rate at which the mesh element size can grow from one element to another (1.4) and varying the maximum side length between d/20 and d/100. Mesh size-independent results are obtained with maximum mesh size equal or lower than d/80, that is thus adopted.

The materials considered here for the model structure are Al and paraffin $C_{18}H_{38}$, with the properties given in paragraph 3 at melting temperature (300K), even if the results on

permeability are not affected by the porous material as well as by the fluid filling it. Simulated tests are carried out to calculate K for several values of ε in the range 0.69-0.99. In some cases, the side length of the model is varied to 5mm to check the independence of K from L. Further, the relevance of calculated K on the PCM composite thickness is carried out by repeating selected simulations for different numbers of stacked cells in the direction of heat flow.

4.2 Effect of side-length on the permeability of (inverse) BCC cells

From each K, the corresponding K'∞ (K'∞ refers to K' obtained when a periodic boundary condition is set) is derived and plotted in Fig. 7 as a function of the porosity ε. The results show that the normalized permeability varies with porosity for BCC structure and confirm the independency of the normalized permeability from cell side, and thus from structure coarseness.

In the same figure the simulated tests results have been compared to experimental data. These latter have been derived for different porosity but two pore diameter values: 75 μm and 400 μm. On the contrary, simulated results have been obtained for coarser structures with fixed side lengths (1 mm and 5 mm) and corresponding pore diameters increasing with the porosity. For example, in the case that side length L is fixed at 1mm, d=925 μm for ε=0.8, and d=976 μm for ε=0.9. Pore diameters for L=5 mm are 5 times those for L=1mm for a given porosity The same plot also shows the other DS results obtained for BCC structures [10,12] (unknown pore diameter or unit cell side). The agreement of all these data is clearly visible.

A best-fit of the above data for low permeability has been performed using the correlation K'∞ =C*(ε-D)E proposed by Ngo and Byon [12] for simple cubic, BCC, FCC structures with ε<0.90. Since the fitting parameters are not specifically mentioned for each lattice type, but only ranges for them are given (0.063<C<0.265, 0.523<D<0.726, 1.531<E< 1.994), the authors of the present paper have identified these parameters for BCC lattice by best-fitting simulation data of normalized permeability (plotted as black line in Fig.7) for ε < 0.90. The following equation has been derived:

$$K'_{\infty} = 0.09|\varepsilon - 0.68|^{1.6} \qquad \text{for } 0.6802<\varepsilon<0.9395 \qquad (21)$$

In Fig.7, it is observed that Eq.21 can well predict K'∞ for the porosity up to about 0.94 and the statistical analysis shows coefficient of determination (R^2) to be 0.997 by comparing results predicted by DS and Eq.21 for 0.69<ε<0.939. But the above analytical description of K'∞ is

clearly unsuitable for the porosity over 0.94, the one which is of more interest for composite PCMs.

Thus, the authors have used two different best fit equations, one considering the whole set of simulated results, the other only for porosity exceeding 0.94. The resulting equations are the following ones, and they are plotted as red and green lines in including all the simulated test results.

$$K'_{\infty} = 131.5237\varepsilon^3 - 376.2025\varepsilon^2 + 358.8131\varepsilon - 114.103 \quad \text{for } 0.9395<\varepsilon<0.9945 \qquad (22)$$

$$K'_{\infty} = 16.0594\varepsilon^4 - 52.4791\varepsilon^3 + 64.1654\varepsilon^2 - 34.7482\varepsilon + 7.0274. \quad \text{for } 0.6802<\varepsilon<0.9945 \qquad (23)$$

By the statistical analysis of results predicted by Eq.22 and DS method for about $0.94<\varepsilon<0.99$, R^2 reaches 0.999. Over the entire porosity considered in Fig.7, Eq.23 can well predict K'_{∞} for the porosity down to about 0.75, even though the statistical analysis show coefficient of determination (R^2) to be 0.992. In the present paper, a combination of Eq.21 for low porosity range and Eq.22 for high porosity range, and a single Eq.23 for a wide porosity range are both applied to estimate K'_{∞} for an inverse BCC lattice structure.

4.3 Effect of the height of PCM composite

The previous calculations of the normalized permeability of the inverse BCC cell structure consider a periodic boundary condition, and thus fluid moves across a porous structure of theoretically infinite height, where no edge conditions occur. In the case of finite-thickness of the porous material filled with liquid, specifically in those characterized by coarse structures, the impossibility to have liquid movement across the external boundary could potentially affect the convective movement of the liquid and thus different permeability could be considered. The present part of the study is aimed at checking if and to what extent normalized permeability is affected by specimen thickness, here considered as the number of stacked unit cells. The geometrical models for DS simulations in this case include several stacked unit cells, and pressure difference is set at the external inlet and outlet surface instead of periodic boundary condition. The normalized permeability is derived from numerical tests results as analogously to what described in paragraph 4.1. Some sets of simulated tests are carried out in the cases that number of stacked cells n equal to 1, 3, 7, 9, 11, 15, 20, 30, varying the porosity between 0.70 and 0.96, where L is fixed at 1mm. In some cases, L= 5mm is additionally considered.

The results of these sets are shown in Fig.8a. Here, the ratio between the calculated K'_n and K'_∞ is given in ordinate, where K'_n represents the K' calculated for n stacked cells (with given ε and L) and K'_∞ is the one calculated for the same ε and L from the simulations presented in paragraph 4.2. Datasets for different porosity values (and in some case both for L=1 mm and L=5 mm) are plotted versus the number of stacked cells. It can be easily noticed that, as expected, for high n the value of K'_n/K'_∞ tends to 1. On the other hand, porosity affects the ratio K'_1/ K'_∞, i.e. the ratio between the K' value when the thickness of the porous structure is equal to the side length of a unit cell and the K'_∞ obtained considering periodic boundary condition. As porosity increases from 0.7 to 0.96, K'_1/ K'_∞ increases only from 1.0013 to 1.0133. The effect of cell size is checked for a relatively critical case of 0.9, and it is found to be negligible (see Fig. 8a). Porosity further affects the number of stacked cells above which the K'_n can be considered as constant. As a matter of fact this value of n increases with ε, being close to 5 stacked cells for ε=0.7, 15 stacked cells for ε=0.96.

The deviation of K'_n from K'_∞ is in any case quite limited,in most cases lower than 1%. The maximum relative error considering K'_∞ instead of K'_n occurs for n=1 and can be easily computed for cells of the same geometry (ε and L) is calculated (in percentage) as:

$$\delta = 100 \times |K'_\infty - K'_1| / K'_1 \qquad (24)$$

The corresponding values for L=1 mm (and in some cases for L=5 mm) are plotted in Fig. 8b. It can be observed that δ increases with porosity. The maximum relative error δ is in any case lower than 1.4%. This means that the error committed considering the thickness-independent values and the normalized permeability model presented in paragraph 4.2 are lower than 1.4% if the ratio between the thickness of the porous medium and L is close to 1.

4.4 Modelled material dependant term $K\times H$ in $\mathbb{R}_D$ equation

As a result, from the analyses of DS results performed in previous paragraphs 4.2 and 4.3, the geometry-only dependent term to be inserted in the equation to calculate the $\mathbb{R}_D$ number can be well approximated by following analytically descriptions:

$$KH = K'_\infty \times d^2 \times H \qquad (25)$$

While Eq. 21-23 supply analytical descriptions in terms of $K'_\infty = K'_\infty(\varepsilon)$ for different porosity ε ranges. On the basis of the geometry relationship d/L=f(ε) for inverse BCC cell as discussed previously, the equation (25) can be written in terms of H, porosity ε, side length L of the BCC

lattice. The description of the geometry-dependent term in $\mathbb{R}_D$ number is here presented in terms of the length L of the inverse BCC structure considering analytical descriptions Eq.23 for K'$_\infty$ and Eq.8 for ratio d/L:

$$KH = K'_\infty d^2 H = (16.0594\varepsilon^4 - 52.4791\varepsilon^3 + 64.1654\varepsilon^2 - 34.7482\varepsilon + 7.0274) \times (4.969\varepsilon^3 - 11.683\varepsilon^2 + 9.599\varepsilon - 1.825)^2 L^2 H \quad (26)$$

Further, many available geometrical data for open cell porous structures are supplied characterizing the material coarseness by means of the parameter pores per inch (PPI). When an inverse BCC structure is considered, the correlation between L and PPI is the following [11]:

$$L\,[mm] = 25.4/PPI. \quad (27)$$

The geometry-dependent term for $\mathbb{R}_D$ number calculation can thus be expressed in terms of PPI and ε (to be used in the range as 0.75<ε <0.96) as:

$$KH = (16.0594\varepsilon^4 - 52.4791\varepsilon^3 + 64.1654\varepsilon^2 - 34.7482\varepsilon + 7.0274) \times (4.969 * \varepsilon^3 - 11.683 * \varepsilon^2 + 9.599 * \varepsilon - 1.825)^2 \times (0.0254/PPI)^2 \times H \quad (28)$$

5 Modelled $\mathbb{R}_D$ number for Al/Paraffin PCM

For a PCM composite formed by an Al porous structure and a paraffin with melting temperature in the range 280-340K, $\mathbb{R}_D$ number can be calculated by combining Eq. 15 with Eq. 26 (or , alternatively, 28), as follows:

$$\mathbb{R}_D = \frac{209.5g\left((\rho Cp)_{Met}(1-\varepsilon)+(\rho Cp)_{paraffin}\varepsilon\right)\left(16.0594\varepsilon^4-52.4791\varepsilon^3+64.1654\varepsilon^2-34.7482\varepsilon+7.0274\right)\left(4.969\varepsilon^3-11.683\varepsilon^2+9.599\varepsilon-1.825\right)^2\Delta THL^2}{T_m*\left(\lambda_{Met}(1-\varepsilon)^{1.3296}+\varepsilon\,\lambda_{paraffin}\right)*\left(38.78\times\exp\left(-18.83\left(\frac{T}{T_b}\right)\right)+0.01426\times\exp\left(-4.329\left(\frac{T}{T_b}\right)\right)\right)} \quad (29)$$

A simplified and approximated equation considered constant-Al phase properties, and density, C_p and thermal conductivity of paraffin at its melting temperature can be obtained combining Eq. (18) with Eq. 26 (or, alternatively, 28).

$$\mathbb{R}_D = \frac{209.5g\left(2452990(1-\varepsilon)+778.2\left(6.33\times10^{-3}\,T_m^2-1.03\,T_m+1961\right)\varepsilon\right)\left(16.0594\varepsilon^4-52.4791\varepsilon^3+64.1654\varepsilon^2-34.7482\varepsilon+7.0274\right)*\left(4.969\varepsilon^3-11.683\varepsilon^2+9.599\varepsilon-1.825\right)^2\Delta THL^2}{T_m*\left(253.9(1-\varepsilon)^{1.3296}+\varepsilon*\left(0.07128\times\left(\frac{T_m}{Tb}\right)^2-0.2056\times\left(\frac{T_m}{Tb}\right)+0.2348\right)\right)\left(38.78\times\exp\left(-18.83\left(\frac{T}{T_b}\right)\right)+0.01426\times\exp\left(-4.329\left(\frac{T}{T_b}\right)\right)\right)} \quad (30)$$

where, as usual, T_b is calculated using Eq. 10.

The above equations supply good description of $\mathbb{R}_D$ for the porosity range $0.75<\varepsilon<0.9945$ since Eq.26 is based on Eq.23 well predicting K'_∞ for the porosity larger than 0.75. For the same porosity range, similar equations can be written combining Eq. 15 or 18 with Eq. 28, when the structure coarseness of the Al porous structure is given in terms of PPI.

5.1 Conditions for conduction-dominant heat transport

Once $\mathbb{R}_D$ is modelled, it is possible to calculate if the conditions for conduction-dominant heat transport are satisfied or not (and natural convection occurs) for a specific Al/paraffin PCM composite. As mentioned in the introduction, natural convection for the liquid paraffin can occur as $\mathbb{R}_D$ overcomes critical $\mathbb{R}_D$ values, here referred as $\mathbb{R}_{DC}$. $\mathbb{R}_{DC}$ is related to heating location. Specifically, critical $\mathbb{R}_D$ values $\mathbb{R}_{DC,\perp}$ is about 40 for heat supplied from the horizontal bottom surface of the composite material [31,33] and $\mathbb{R}_{DC,\vdash}$ =1 can be considered for heat supplied horizontally from one lateral vertical surface of the PCM composites [32] .

The conditions where conduction-dominant heat transport occurs can be thus obtained focusing on several geometrical or material parameters (such as the cell coarseness L, the porosity ε, the specimen thickness H), by rearranging Eq.29 (or its simplified version, Eq.30). A similar approach could be followed by considering the selection of different paraffins, characterising them in terms of their melting temperature T_m. The above equations are the ones valid for the wider porosity range. Better description for high- and low- porosity ranges can be obtained by using the corresponding analytical description of K'_∞ (i.e., Eq.21 and Eq.22) into the geometry-dependent term for $\mathbb{R}_D$ estimation.

For the case of length, the condition for conduction-dominant cases is when L is lower than the critical value L_c, the most general equation is:

$$L < Lc = \sqrt{\frac{\mathbb{R}_{DC} T_m \left(\lambda_{Met}\,(1-\varepsilon)^{1.3296} + \varepsilon\,\lambda_{paraffin}\right) \times \left(38.78 \times \exp\left(-18.83\left(\frac{T}{T_b}\right)\right) + 0.01426 \times \exp\left(-4.329\left(\frac{T}{T_b}\right)\right)\right)}{209.5\,g\left((\rho Cp)_{Met}(1-\varepsilon) + (\rho Cp)_{paraffin}\varepsilon\right)(16.0594\varepsilon^4 - 52.4791\varepsilon^3 + 64.1654\varepsilon^2 - 34.7482\varepsilon + 7.0274)(\,4.969\varepsilon^3 - 11.683\varepsilon^2 + 9.599\varepsilon - 1.825)^2} \left(\frac{1}{\Delta TH}\right)} \quad (31)$$

While in the case where the thermophysical parameters (λ, ρ and C_p) of Al are constant and those of paraffin are values at its melting temperature, the equation becomes:

$$L = Lc < \sqrt{\frac{\mathbb{R}_{DC} T_m (253.9(1-\varepsilon)^{1.3296} + \varepsilon \times \left(0.07128 \times \left(\frac{Tm}{\mathrm{Tb}}\right)^2 - 0.2056 \times \left(\frac{Tm}{\mathrm{Tb}}\right) + 0.2348\right)) \times \left(38.78 \times \exp\left(-18.83\left(\frac{T}{Tb}\right)\right) + 0.01426 \times \exp\left(-4.329\left(\frac{T}{Tb}\right)\right)\right)}{2055.195\left(2452990(1-\varepsilon) + 778.2\left(6.33 \times 10^{-3}\, {T_m}^2 - 1.03\, T_m + 1961\right)\varepsilon\right)(16.0594\varepsilon^4 - 52.4791\varepsilon^3 + 64.1654\varepsilon^2 - 34.7482\varepsilon + 7.0274)(\,4.969\varepsilon^3 - 11.683\varepsilon^2 + 9.599\varepsilon - 1.825)^2} \left(\frac{1}{\Delta TH}\right)}$$

(32)

Where, as usual, T_m and T_b (derived by Eq. 10) and ΔT are given in K, H and L are given in m, and ε (porosity) corresponds to the volume fraction of the paraffins used as PCM.

A reference condition is considered for the case of horizontal heating ($\mathbb{R}_{DC}$=1), the low-melting paraffin $C_{18}H_{38}$ (T_m=300 K), H=25 mm and ΔT =10 K, with the surface opposite to the heated one at T_m. The correlation between the critical length L_c and the porosity ε can be derived from the simplified Eq. 32, considering the temperature T (to estimate dynamic viscosity at $T_m+\Delta T$) and plotted as black lines in Fig. 9a-9c. For comparison purposes, lines corresponding to data calculated using the high- and low porosity equations (Eq.21 and Eq.22) for K'_∞ are drawn as dashed lines. These three figures further represent the case where the paraffin types, the height of PCM composite, or the temperature difference across it are varied, respectively. Fig. 9a shows that, for relatively high porosity range (ε above 0.9) and for the thickness of 25 mm and ΔT =10 K, there is no convection motion for all the considered paraffin if the length of the unit cell is smaller than 1.3 mm (about 20 PPI), to be read in the right-side vertical axis. It is also clear that the approximated description of K'_∞ does not predict good L_c for porosity lower than 0.75, where K'_∞ is low and the discrepancy between its values obtained using single- or two-range for ε is relatively high. On the contrary, for the low porosity porous material (i.e., lower than 0.75), where the molten filling material can be considered as almost trapped into isolated spheres, the structure coarseness range where the heat transfer is conductive increases a lot (up to L=6 mm, corresponding to less than about 4 PPI). The direct correlation of Lc (1/H) is clearly visible in Fig. 9b, where reduces for an increase of H from 5 mm to 50 mm.

The effect of ΔT, shown in Fig. 9c, is similar to that of H since the correlation between L_c and H or ΔT is the same. It can be further observed that Eq. 32 can be rearranged considering the average temperature gradient $\Delta T/H$ (assumed to be constant along the thickness) instead of the temperature difference ΔT. The results from part of the second and third set data (given in Fig. 9b and 9c) are presented in terms of the average temperature gradients $\Delta T/H$ in Fig.9d, only considering the single-range simplified Eq. 32 for porosity values exceeding 0.75.

The reference condition used to draw plots in Figure 9 considers the specimens heated on a lateral surface, thus $\mathbb{R}_{DC}$ equals to1. Similar evaluations of the combined effects of porosity, paraffin type and ΔT could be obtained for different heating by inserting proper $\mathbb{R}_{DC}$ (such as the abovementioned value close to 40 in the case of specimens heated from the bottom).

5.2 Validation of the simplified model for $\mathbb{R}_D$ number calculation

Experimental data available from literature [25] have been used to validate the model with single-porosity range description of K'_{∞} (Eq. 32). These values refer to composite PCMs made by pure Al foams (their stated thermal conductivity is 236 W/(m·K)) which have been filled by a paraffin stated to melt at about 300K (T_m close to that of the paraffin $C_{18}H_{38}$). Two sets of composite PCM samples, all having the same size 101.6 mm ×101.6 mm×50.8 mm, confined laterally by insulated plates. The first set is characterized by the same pore coarseness (10 PPI) and different porosity (0.884, 0.934, 0.966). The second set is characterized by a constant porosity of about 0.936 and different PPI (10, 20, 40). The samples were heated with constant power on their square surface, placed vertically and the temperature at several location from the heated to the opposite surfaces were measured and the temperature profiles were given in the paper. Thus, the model was applied here considering $\mathbb{R}_{DC}$ equal to 1. The possibility to observe the melting interface, due to the paraffin feature changing from opaque to transparent as melting occurs was used by Lafdi et al. [25]. The representative results of the tests [25] are shown in Fig.10. Among the experimental specimens, the first one shown here exhibits the strong natural convection. The specimen, when heater is on the left surface, where the solid/liquid profile inclined rightward in its upper part means that convection is taking place.

In order to carry out the validation of the model described by Eq. 32, the identification of the temperatures and H is needed for each specimen. The temperature on the vertical, heated surface is derived from temperature profiles at the (different) time at which macrographs of the samples were taken by Lafdi et al. [25]. This temperature is used to calculate ΔT as the difference between it and T_m. In the experimental tests, the previously described specimen thickness cannot be considered as the one used to derive L_c-ε correlation, since the molten liquid does not fill the whole thickness. Thus, for the 6 specimens for which the solid/liquid interfaces are available, H is considered as the distance between the external heating surface and the solid/liquid interface at the height level where the profile changes from vertical to inclined (see examples in Fig. 10). The H values derived in this way, as well as the ΔT are given for each experimental test in the legend of Fig. 11, where experimental points corresponding to each specimen are placed in terms of their PPI and porosity. Further, Fig. 11 shows the curves for L_c calculated on the basis of H and the ΔT for each sample, adopting the same colour. Thus, for the two specimens with the same porous structure characteristics (10 PPI and porosity 0.934) two L_c curves are derived, each corresponding to an experimental test. The presence of convection in each test can be compared to the position of the corresponding line. Most of the points lay above the corresponding curves, and convection is actually

observed by Lafdi et al. [25]. For them, the solid-liquid interface is more inclined as the relative distance between points and the corresponding line increases. Convection motion is predicted and experimentally demonstrated not to occur for the sample of set 1 with the lowest porosity (black point and line). Lastly, for the sample of set 2 with the highest PPI (lowest L), the point is only slightly above the corresponding L_c line, meaning convection motion is quite weak. Also, this situation corresponds to experimental observations.

As a result, the experimental tests by Lafdi et al [25] validate the model for calculation of conditions leading onset of convection (or, alternatively, for conduction-dominant heat transfer) for Al/paraffin composites.

6 Conclusion

The composite PCMs considered in the present paper are formed by paraffins with open-cell metallic Al porous foam which has been modelled as a (inverse) body-centred cubic (BCC) lattice. Analytical expressions have been given to correlate porosity with side length, pore diameter or pores per inch for this structure.

Further, analytical expression has been proposed to model the effective thermal conductivity of the composite PCMs, indirectly based on the melting temperature of the PCM. The BCC structure has been proved to be the most suitable to model this property for Al foams with high porosity.

The Rayleigh Darcy ($\mathbb{R}_D$) number can be obtained as a product of the temperature difference, the material-dependent term M and the geometry-dependent term (KH). M has been analytically described by a general version or a simplified one, and (KH) also has been analytically calculated for different porosity ranges for composite PCMs. With respect to previous analytical models for permeability for porosity less than 0.94, the description adopted here has been proved to be suitable also for porosity in the 0.94-0.99 range.

The above equations are used to calculate critical conditions for conduction-dominant heat transfer of the paraffin within a metallic foam when heated horizontally. Specifically, the model has been rearranged to predict the porous structure coarseness (in terms of L or PPI) leading to natural convection for the different porosity, thickness of specimen containing molten paraffin, its temperature range and paraffin types. A graphical procedure is suggested to check the onset of natural convection, which is adopted to validate the simplified model by the experimental

results for several Al open-cell foams filled with specific paraffin. They have a good agreement.

The supplied equations and plots for critical conditions derived for horizontal heating can be easily modified for the case of heating from the bottom of the material (in this case L_c is about 6.3 times the one presented in this paper). The approach used here can be further extended to different composite materials containing a liquid phase and an open-cell porous structure, with a simple definition of M term.

Acknowledgements

This work was supported by the Italian Ministry for Education, University and Research through the project Department of Excellence LIS4.0 (Integrated Laboratory for Lightweight and Smart Structures).

Reference

[1] K. Pielichowska, K. Pielichowski, Phase change materials for thermal energy storage, Prog. Mater. Sci. 65 (2014) 67–123. doi:10.1016/j.pmatsci.2014.03.005.

[2] H. Nazir, M. Batool, F.J. Bolivar Osorio, M. Isaza-Ruiz, X. Xu, K. Vignarooban, P. Phelan, Inamuddin, A.M. Kannan, Recent developments in phase change materials for energy storage applications: A review, Int. J. Heat Mass Transf. 129 (2019) 491–523. doi:10.1016/j.ijheatmasstransfer.2018.09.126.

[3] P. Sobolciak, M. Karkri, M.A. Al-Maadeed, I. Krupa, Thermal characterization of phase change materials based on linear low-density polyethylene, paraffin wax and expanded graphite, Renew. Energy. 88 (2016) 372–382. doi:10.1016/j.renene.2015.11.056.

[4] G. Wang, G. Wei, C. Xu, X. Ju, Y. Yang, X. Du, Numerical simulation of effective thermal conductivity and pore-scale melting process of PCMs in foam metals, Appl. Therm. Eng. 147 (2019) 464–472. doi:10.1016/j.applthermaleng.2018.10.106.

[5] H. JianShe, Y. Chao, Z. Xu, Z. Jiao, D. JinXing, Structure and thermal properties of expanded graphite/paraffin composite phase change material, Energy Sources, Part A Recover. Util. Environ. Eff. 41 (2019) 86–93. doi:10.1080/15567036.2018.1496199.

[6] W. Li, Y. Dong, X. Zhang, X. Liu, Preparation and Performance Analysis of Graphite Additive/Paraffin Composite Phase Change Materials, Processes. 7 (2019) 447.

661 doi:10.3390/pr7070447.

662 [7] Y. Yao, H. Wu, Thermal transport process of metal foam/paraffin composite (MFPC)
663 with solid-liquid phase change: An experimental study, Appl. Therm. Eng. 179 (2020)
664 115668. doi:10.1016/j.applthermaleng.2020.115668.

665 [8] Z. Tao, H. Wang, J. Liu, W. Zhao, Z. Liu, Q. Guo, Dual-level packaged phase change
666 materials – thermal conductivity and mechanical properties, Sol. Energy Mater. Sol.
667 Cells. 169 (2017) 222–225. doi:10.1016/j.solmat.2017.05.030.

668 [9] W. Xu, H. Zhang, Z. Yang, J. Zhang, The effective thermal conductivity of three-
669 dimensional reticulated foam materials, J. Porous Mater. 16 (2009) 65–71.
670 doi:10.1007/s10934-007-9169-4.

671 [10] S. Krishnan, J.Y. Murthy, S. V. Garimella, Direct Simulation of Transport in Open-
672 Cell Metal Foam, J. Heat Transfer. 128 (2006) 793–799. doi:10.1115/1.2227038.

673 [11] L. Zhang, X. Zhang, Z. Liu, An Efficient Numerical Method for Pressure Loss
674 Investigation in an Oil/Air Separator with Metal Foam in an Aero-Engine, Energies. 13
675 (2020) 346. doi:10.3390/en13020346.

676 [12] I.-L. Ngo, C. Byon, Permeability of microporous wicks with geometric inverse to
677 sintered particles, Int. J. Heat Mass Transf. 92 (2016) 298–302.
678 doi:10.1016/j.ijheatmasstransfer.2015.08.040.

679 [13] X. Sun, Q. Zhang, M.A. Medina, K.O. Lee, Experimental observations on the heat
680 transfer enhancement caused by natural convection during melting of solid–liquid
681 phase change materials (PCMs), Appl. Energy. 162 (2016) 1453–1461.
682 doi:10.1016/j.apenergy.2015.03.078.

683 [14] P. Ternik, R. Rudolf, Heat transfer enhancement for natural convection flow of water-
684 based nanofluids in a square enclosure, Int. J. Simul. Model. 11 (2012) 29–39.
685 doi:10.2507/IJSIMM11(1)3.198.

686 [15] R. Pakrouh, M.J. Hosseini, A.A. Ranjbar, A parametric investigation of a PCM-based
687 pin fin heat sink, Mech. Sci. 6 (2015) 65–73. doi:10.5194/ms-6-65-2015.

688 [16] P.T. Sardari, H.I. Mohammed, D. Giddings, G.S. Walker, M. Gillott, D. Grant,
689 Numerical study of a multiple-segment metal foam-PCM latent heat storage unit:
690 Effect of porosity, pore density and location of heat source, Energy. 189 (2019)

116108. doi:10.1016/j.energy.2019.116108.

[17] A.A. Rabienataj Darzi, M. Jourabian, M. Farhadi, Melting and solidification of PCM enhanced by radial conductive fins and nanoparticles in cylindrical annulus, Energy Convers. Manag. 118 (2016) 253–263. doi:10.1016/j.enconman.2016.04.016.

[18] J. Xie, K.F. Choo, J. Xiang, H.M. Lee, Characterization of natural convection in a PCM-based heat sink with novel conductive structures, Int. Commun. Heat Mass Transf. 108 (2019) 104306. doi:10.1016/j.icheatmasstransfer.2019.104306.

[19] M. Ghalambaz, A.J. Chamkha, D. Wen, Natural convective flow and heat transfer of Nano-Encapsulated Phase Change Materials (NEPCMs) in a cavity, Int. J. Heat Mass Transf. (2019). doi:10.1016/j.ijheatmasstransfer.2019.04.037.

[20] M. Ghalambaz, S.A.M. Mehryan, I. Zahmatkesh, A. Chamkha, Free convection heat transfer analysis of a suspension of nano–encapsulated phase change materials (NEPCMs) in an inclined porous cavity, Int. J. Therm. Sci. (2020). doi:10.1016/j.ijthermalsci.2020.106503.

[21] H. Zheng, C. Wang, Q. Liu, Z. Tian, X. Fan, Thermal performance of copper foam/paraffin composite phase change material, Energy Convers. Manag. 157 (2018) 372–381. doi:10.1016/j.enconman.2017.12.023.

[22] Y. Tian, C.Y. Zhao, A numerical investigation of heat transfer in phase change materials (PCMs) embedded in porous metals, Energy. 36 (2011) 5539–5546. doi:10.1016/j.energy.2011.07.019.

[23] X. Hu, H. Wan, S.S. Patnaik, Numerical modeling of heat transfer in open-cell micro-foam with phase change material, Int. J. Heat Mass Transf. 88 (2015) 617–626. doi:10.1016/j.ijheatmasstransfer.2015.04.044.

[24] S.M. Hashem Zadeh, S.A.M. Mehryan, M. Ghalambaz, M. Ghodrat, J. Young, A. Chamkha, Hybrid thermal performance enhancement of a circular latent heat storage system by utilizing partially filled copper foam and Cu/GO nano-additives, Energy. 213 (2020) 118761. doi:10.1016/j.energy.2020.118761.

[25] K. Lafdi, O. Mesalhy, S. Shaikh, Experimental study on the influence of foam porosity and pore size on the melting of phase change materials, J. Appl. Phys. 102 (2007) 083549. doi:10.1063/1.2802183.

[26] M. Caliano, N. Bianco, G. Graditi, L. Mongibello, Analysis of a phase change material-based unit and of an aluminum foam/phase change material composite-based unit for cold thermal energy storage by numerical simulation, Appl. Energy. 256 (2019) 113921. doi:10.1016/j.apenergy.2019.113921.

[27] B. Buonomo, H. Celik, D. Ercole, O. Manca, M. Mobedi, Numerical study on latent thermal energy storage systems with aluminum foam in local thermal equilibrium, Appl. Therm. Eng. 159 (2019) 113980. doi:10.1016/j.applthermaleng.2019.113980.

[28] H.M. Sadeghi, M. Babayan, A. Chamkha, Investigation of using multi-layer PCMs in the tubular heat exchanger with periodic heat transfer boundary condition, Int. J. Heat Mass Transf. (2020). doi:10.1016/j.ijheatmasstransfer.2019.118970.

[29] A. Chamkha, A. Veismoradi, M. Ghalambaz, P. Talebizadehsardari, Phase change heat transfer in an L-shape heatsink occupied with paraffin-copper metal foam, Appl. Therm. Eng. (2020). doi:10.1016/j.applthermaleng.2020.115493.

[30] A.I. Alsabery, R. Mohebbi, A.J. Chamkha, I. Hashim, Effect of local thermal non-equilibrium model on natural convection in a nanofluid-filled wavy-walled porous cavity containing inner solid cylinder, Chem. Eng. Sci. (2019). doi:10.1016/j.ces.2019.03.006.

[31] E.B. Soboleva, Rayleigh-Darcy convection in a porous layer: A comparison of near-critical and normal fluid phases, ArXiv Prepr. ArXiv1001.4139. (2010).

[32] D. Poulikakos, Unsteady natural convection in a porous layer, Phys. Fluids. 26 (1983) 1183. doi:10.1063/1.864266.

[33] L.E. Howle, Convection in Ordered and Disordered Porous Layers, in: D.B. Ingham, I.B.T.-T.P. in P.M.I.I. Pop (Eds.), Transp. Phenom. Porous Media II, Elsevier, Oxford, 2002: pp. 155–176. doi:10.1016/B978-008043965-5/50007-6.

[34] Z. Li, E. Gariboldi, Review on the temperature-dependent thermophysical properties of liquid paraffins and composite PCMs with metallic porous structures, Mater. Today Energy. (2021) 100642. doi:10.1016/j.mtener.2021.100642.

[35] T. Fiedler, I.V. Belova, A. Rawson, G.E. Murch, Optimized Lattice Monte Carlo for thermal analysis of composites, Comput. Mater. Sci. 95 (2014) 207–212. doi:10.1016/j.commatsci.2014.07.029.

[36] E. Solórzano, J.A. Reglero, M.A. Rodríguez-Pérez, D. Lehmhus, M. Wichmann, J.A. de Saja, An experimental study on the thermal conductivity of aluminium foams by using the transient plane source method, Int. J. Heat Mass Transf. 51 (2008) 6259–6267. doi:10.1016/j.ijheatmasstransfer.2007.11.062.

[37] A. Bhattacharya, V.V. Calmidi, R.L. Mahajan, Thermophysical properties of high porosity metal foams, Int. J. Heat Mass Transf. 45 (2002) 1017–1031. doi:10.1016/S0017-9310(01)00220-4.

[38] R. Singh, H.. Kasana, Computational aspects of effective thermal conductivity of highly porous metal foams, Appl. Therm. Eng. 24 (2004) 1841–1849. doi:10.1016/j.applthermaleng.2003.12.011.

[39] K. Boomsma, D. Poulikakos, On the effective thermal conductivity of a three-dimensionally structured fluid-saturated metal foam, Int. J. Heat Mass Transf. 44 (2001) 827–836. doi:10.1016/S0017-9310(00)00123-X.

[40] V. V. Calmidi, R.L. Mahajan, The Effective Thermal Conductivity of High Porosity Fibrous Metal Foams, J. Heat Transfer. 121 (1999) 466–471. doi:10.1115/1.2826001.

[41] X.H. Yang, J.J. Kuang, T.J. Lu, F.S. Han, T. Kim, A simplistic analytical unit cell based model for the effective thermal conductivity of high porosity open-cell metal foams, J. Phys. D. Appl. Phys. 46 (2013) 255302. doi:10.1088/0022-3727/46/25/255302.

[42] A.J. Rawson, E. Kisi, C. Wensrich, Microstructural efficiency: Structured morphologies, Int. J. Heat Mass Transf. 81 (2015) 820–828. doi:10.1016/j.ijheatmasstransfer.2014.11.012.

[43] X. Xiao, P. Zhang, M. Li, Effective thermal conductivity of open-cell metal foams impregnated with pure paraffin for latent heat storage, Int. J. Therm. Sci. 81 (2014) 94–105. doi:10.1016/j.ijthermalsci.2014.03.006.

[44] Y. Yao, H. Wu, Z. Liu, A new prediction model for the effective thermal conductivity of high porosity open-cell metal foams, Int. J. Therm. Sci. 97 (2015) 56–67. doi:10.1016/j.ijthermalsci.2015.06.008.

[45] M.M. EL IDI, M. KARKRI, M. KRAIEM, Preparation and effective thermal conductivity of a Paraffin/ Metal Foam composite, J. Energy Storage. 33 (2021)

781 102077. doi:10.1016/j.est.2020.102077.

782 [46] R.C. Progelhof, J.L. Throne, R.R. Ruetsch, Methods for predicting the thermal
783 conductivity of composite systems: A review, Polym. Eng. Sci. 16 (1976) 615–625.
784 doi:10.1002/pen.760160905.

785 [47] J. DESPOIS, A. MORTENSEN, Permeability of open-pore microcellular materials,
786 Acta Mater. 53 (2005) 1381–1388. doi:10.1016/j.actamat.2004.11.031.

787

Nomenclature			
d	Diameter of sphere [m]	ε	Porosity [-]
g	Gravitational acceleration [m/s^2]	θ	a fitting constant of Progelhof model [-]
H	Specimen height [m]	λ	thermal conductivity [W/(m·K)]
I	Thermal inertia [kg/(s^2·m·K)]	Abbreviation/subscripts	
K	Permeability [m^2]	∞	infinite value
K'	Normalized permeability [-]	1	one unit cell
L	Side length [m]	⊥	heat supplied from the horizontal bottom surface
L_c	Critical side length [m] for onset of natural convection	BCC	body-centered cubic
M	Material dependent term of RD	c	critical value
M'	Ratio between M at a given temperature and the value of M assumed at the melting temperature of the molten (PCM, paraffin) phase	DS	direct simulation
n	Number of stacked cells	eff	effective value
P	Pressure [Pa]	FCC	face-centred cubic
R^2	Coefficient of determination [-]	high	high-conductivity phase
Re	Reynold number [-]	j	jth phase
T	Temperature [K]	LMC	lattice Monte Carlo
Tb	Boiling temperature [K]	low	low-conductivity phase
Greek symbols		Met	metallic phase of composites

μ	Dynamic viscosity [Pa·s]	NETC	normalized effective thermal conductivity
ρ	Density [kg/m^3]	PCM	phase change material
u	Average velocity of the liquid [m/s]	PPI	pores per inch
α	Thermal diffusivity [m^2/s]	$\mathbb{R}_D$	Rayleigh-Darcy number
β	Coefficient of volumetric thermal expansion [1/K]	SC	simple cubic
δ	maximum relative error considering K'¥ instead of K'$_1$ [-]	TES	thermal energy storage
Δ	Difference	⊦	heat supplied horizontally from one lateral vertical surface

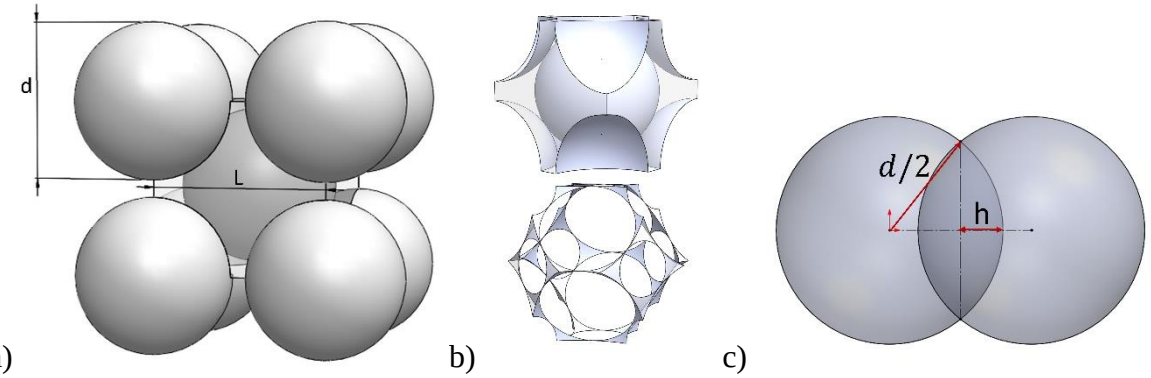

a) b) c)

Figure1 a) Schematic representation of the interconnected spheres in a BCC structure (volume filled by the PCM); b) Al unit inverse BCC cell for the two extreme cases; c) geometrical definition of h.

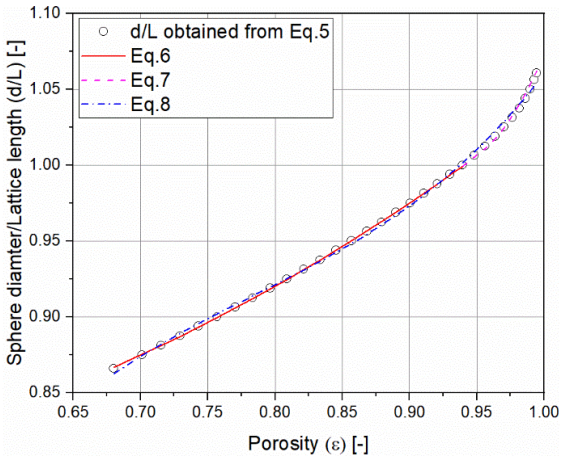

Figure 2 Correlation between porosity ε in (inverse) BCC structure and the sphere diameter to lattice length ratio (d/L). Datapoints refer to data derived from Eq.5, while curves refer to the best fit equations in different porosity ranges (Eq.6-8).

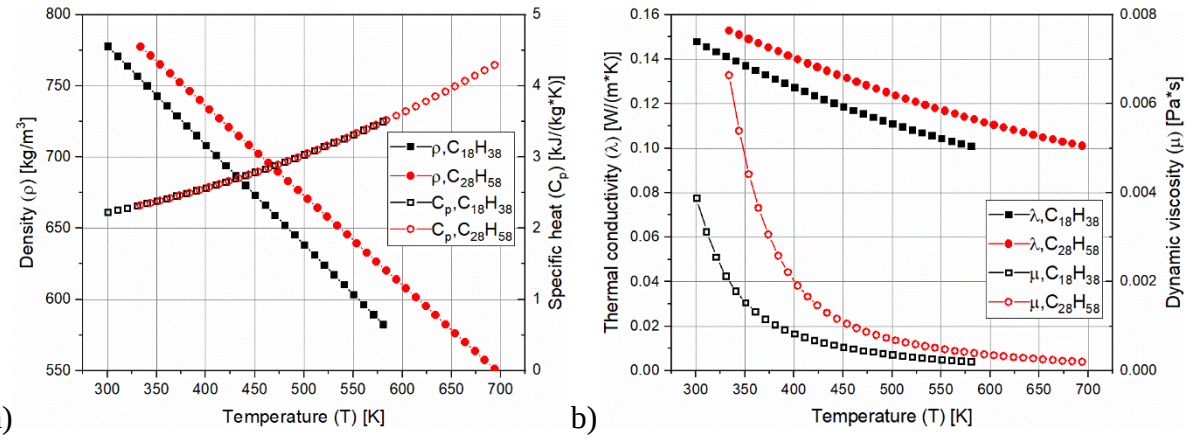

a) b)

Figure 3 Temperature-dependence of thermophysical properties of paraffin $C_{18}H_{38}$ and $C_{28}H_{58}$. a) Density and specific heat; b) Thermal conductivity and dynamic viscosity

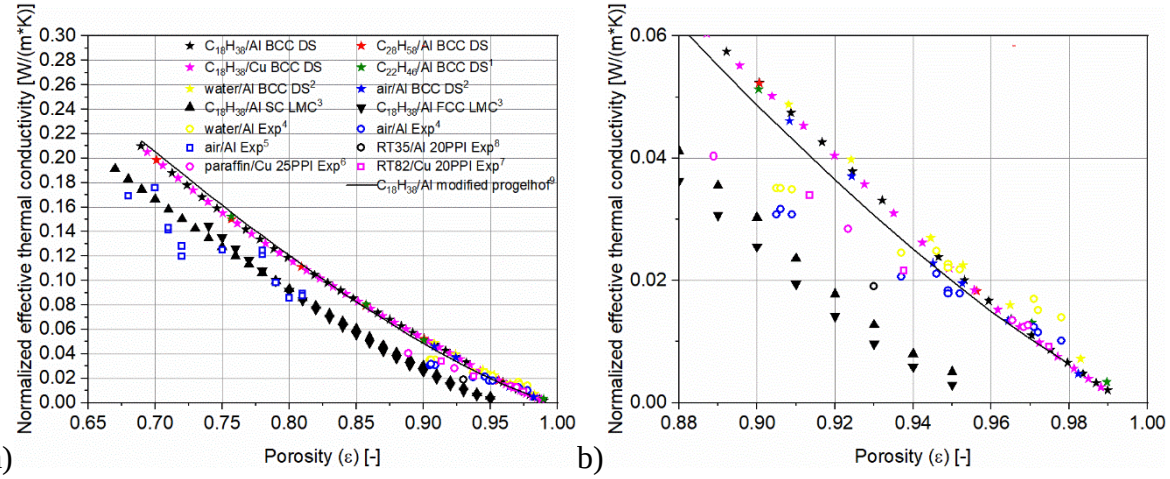

a) b)

Figure 4 Normalized effective thermal conductivity (NETC) of composite structure with an open-cell porous structure at different porosity (volume fraction) ε. Fig. 4b illustrates the data of Fig. 4a in the high porosity- low NETC range. The combinations of paraffins, air or water and the metallic structures used are given in the legend (the same for both plots). The literature works where data have been obtained can be derived from apex numbers as follows: 1 refers to [23], 2 is [10], 3 is [42], 4 is [40], 5 is [36], 6 is [43], 7 is [44], 8 is [45] 9 is [34].

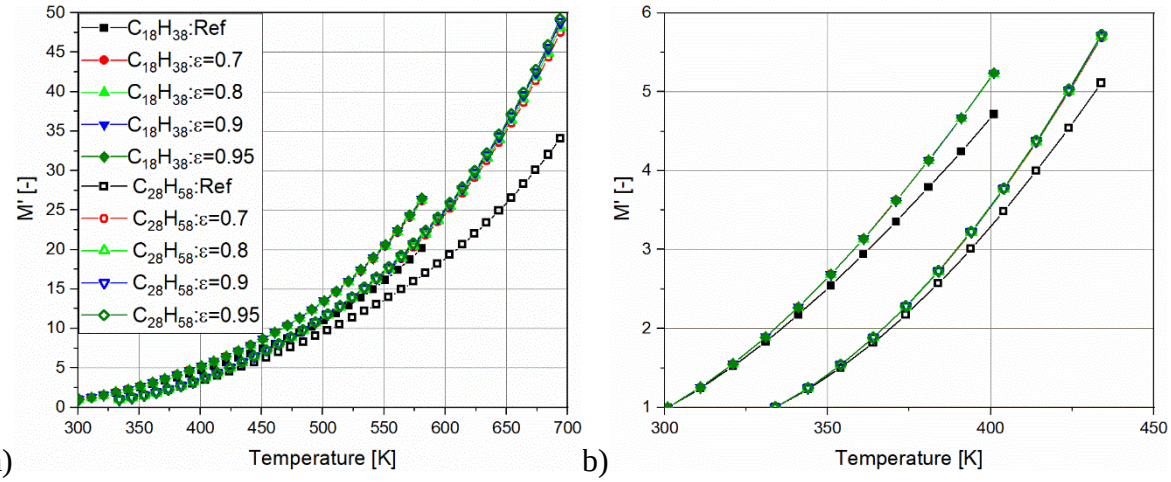

Figure 5 a) Temperature-dependence of material-dependent term M' for composite PCMs formed by paraffins $C_{18}H_{38}$ or $C_{28}H_{58}$ and Al porous structure with porosity in the range 0.7-0.95. Ref corresponds to the case of M' calculated considering all properties constant at T_m with the only temperature-dependence associated with the dynamic viscosity b) Temperature-dependence of the M' in the temperature range from T_m to T_m+100K for $C_{18}H_{38}$ or $C_{28}H_{58}$.

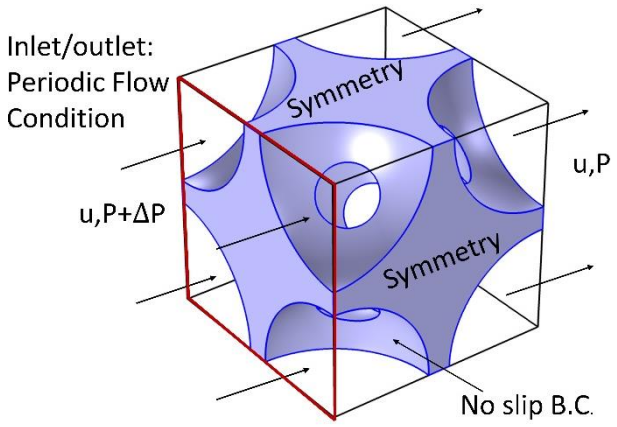

Figure 6 Geometrical model for unit cell of PCM composites used for DS simulation and boundary conditions set to evaluate the permeability K.

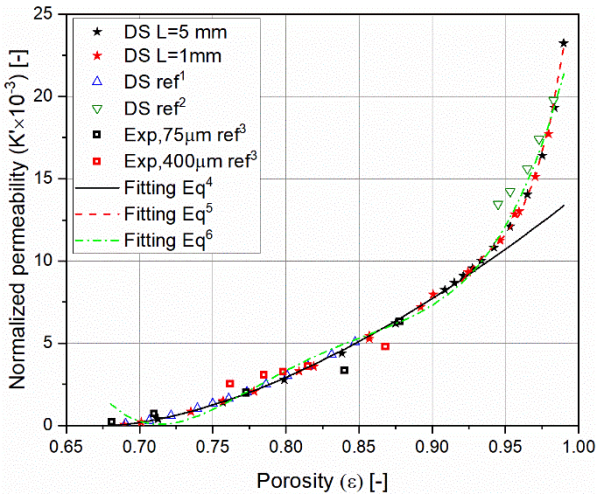

Figure 7. Normalized permeability vs porosity correlation. Datapoints of the present study given in terms of side length L=1 and L=5mm are compared to experimental data for pore diameters 75 μm and 400 μm (3:ref[47]), literature DS results (1: ref[12] 2:ref[10]).The best fit equation 4 refers to Eq.21, 5 is Eq.22, 6 is Eq.23.

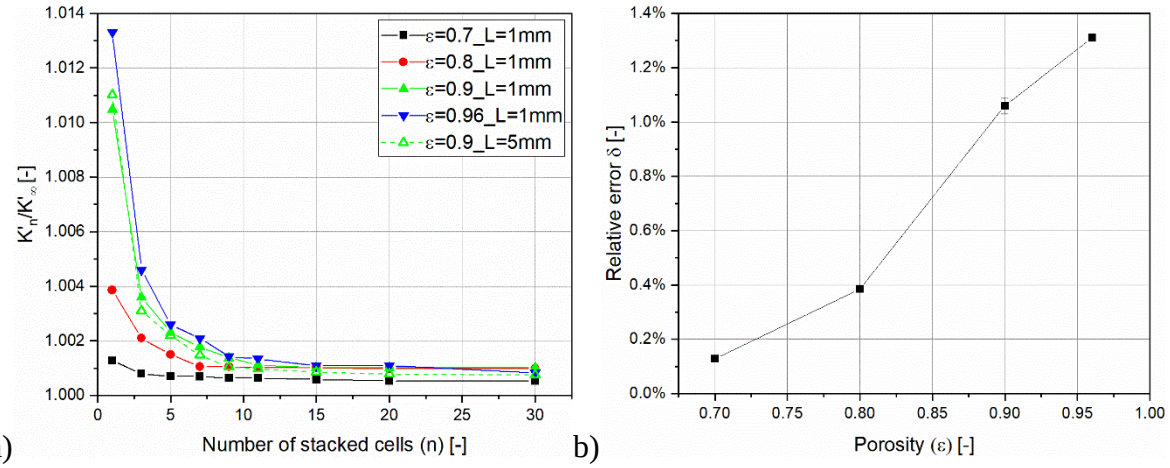

a) b)

Figure 8 Normalized permeability ratio K'_n / K'_∞ vs. number of stacked cells for BCC structure for porosity of 0.7 to 0.96 (a) and relative error δ obtained considering K'_∞ instead of K'_1, representing the maximum relative error for porous structures of finite thickness.

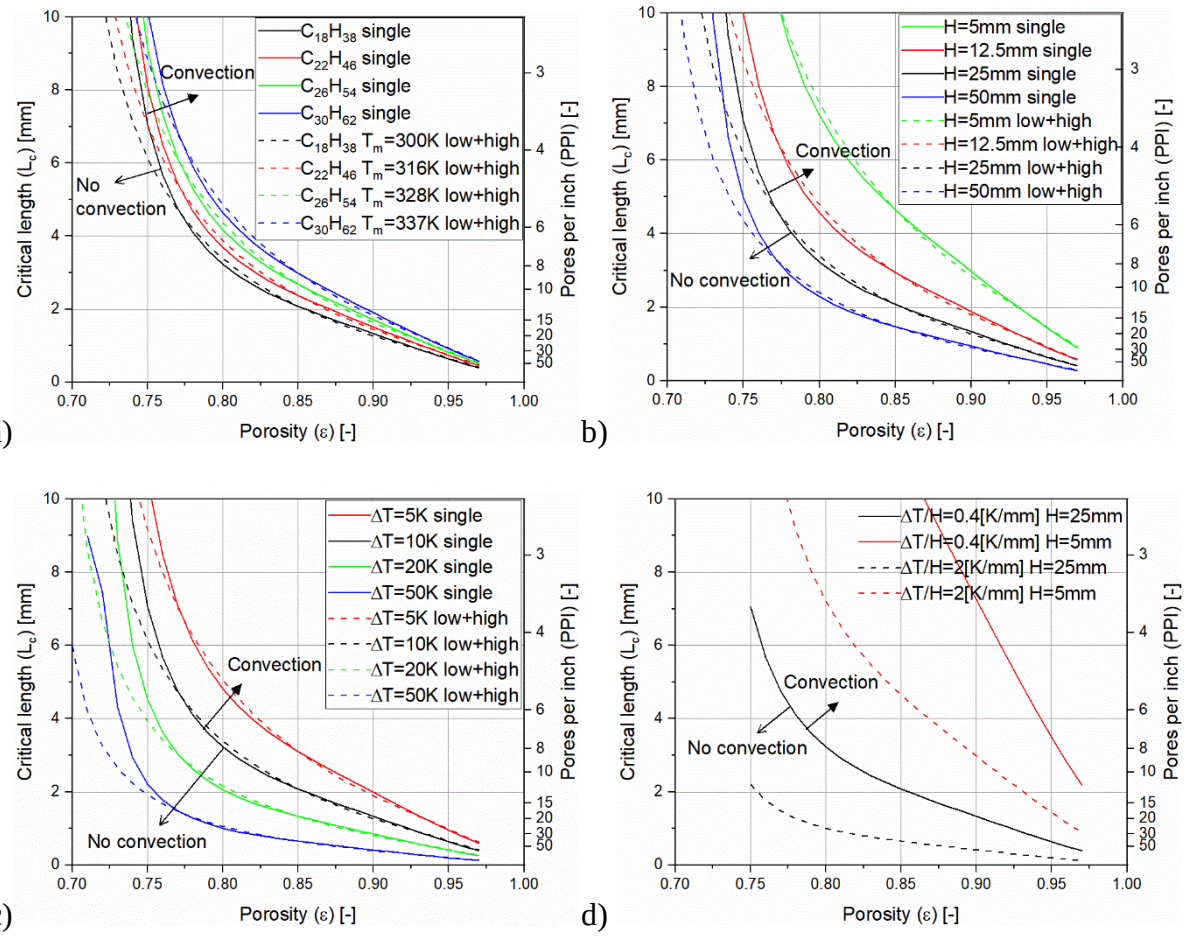

Figure 9 Correlations between the critical length L_c and porosity for a reference case (Al/$C_{18}H_{38}$ paraffin, H=25 mm and ΔT=10 K) in the case of specimen laterally heated are compared to situations where different paraffins (a), different specimen thickness H (b) or different temperature difference across the specimen (c) are set. (d) shows L_c-ε in terms of the average temperature gradient ΔT/H for H=25 mm or 5 mm. In plots a-c lines corresponding to $\mathbb{R}_D$ calculated using K'∞ for a single (wide) range of porosity are plotted in solid lines (referred as 'single' in the legend), those corresponding to K'∞ calculated separately for low-and high-porosity range are plotted as dashed lines (referred as 'low+high' in the legend). Lines in (d) only refer to single range description of K'∞.

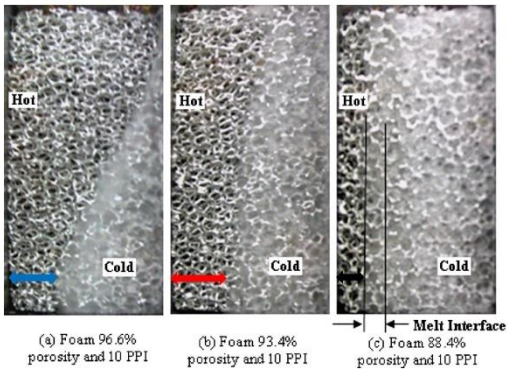

835

836 Figure 10 Set 1 PCM composites experimentally tested by Lafdi et al. (reprinted from [25],
837 with the permission of AIP Publishing) by heating them on vertical surface, shown on the left-
838 side in these images. For each specimen, the distance arrow is added to show how values of H
839 are derived.

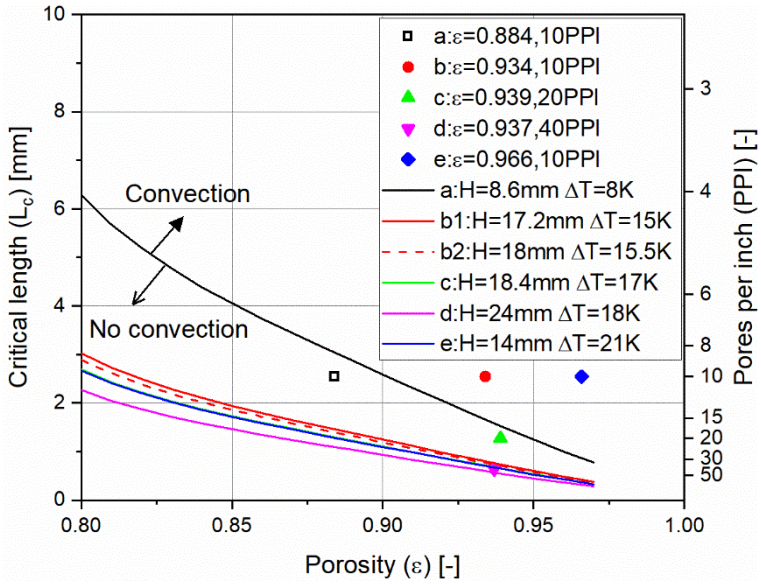

840

841 Figure 11 Correlations between porosity ε and the critical length L_c (or corresponding pore size
842 PPI) above which natural convection occurs for the experimental tests carried out by Lafdi at
843 al. [25], compare to points corresponding to samples with the specific porosity and PPI. The
844 sample with open symbol, laying below the corresponding line, displays no convection.

845